PRAMANA
— journal of
physics

Vol. 60, No. 4
April 2003
pp. 639–650

Heavy ion collisions at collider energies – Insights from PHENIX

A DREES[28], for the PHENIX Collaboration

K Adcox[40], S S Adler[3], N N Ajitanand[27], Y Akiba[14], J Alexander[27], L Aphecetche[34], Y Arai[14], S H Aronson[3], R Averbeck[28], T C Awes[29], K N Barish[5], P D Barnes[19], J Barrette[21], B Bassalleck[25], S Bathe[22], V Baublis[30], A Bazilevsky[12,32], S Belikov[12,13], F G Bellaiche[29], S T Belyaev[16], M J Bennett[19], Y Berdnikov[35], S Botelho[33], M L Brooks[19], D S Brown[26], N Bruner[25], D Bucher[22], H Buesching[22], V Bumazhnov[12], G Bunce[3,32], J Burward-Hoy[28], S Butsyk[28,30], T A Carey[19], P Chand[2], J Chang[5], W C Chang[1], L L Chavez[25], S Chernichenko[12], C Y Chi[8], J Chiba[14], M Chiu[8], R K Choudhury[2], T Christ[28], T Chujo[3,39], M S Chung[15,19], P Chung[27], V Cianciolo[29], B A Cole[8], D G D'Enterria[34], G David[3], H Delagrange[34], A Denisov[12], A Deshpande[32], E J Desmond[3], O Dietzsch[33], B V Dinesh[2], A Drees[28], A Durum[12], D Dutta[2], K Ebisu[24], Y V Efremenko[29], K El Chenawi[40], A Enokizono[11], H En'yo[17,31], S Esumi[39], L Ewell[3], T Ferdousi[5], D E Fields[25], S L Fokin[16], Z Fraenkel[42], A Franz[3], A D Frawley[9], S-Y Fung[5], S Garpman[20,*], T K Ghosh[40], A Glenn[36], A L Godoi[33], Y Goto[32], S V Greene[40], M Grosse Perdekamp[32], S K Gupta[2], W Guryn[3], H-Å Gustafsson[20], T Hachiya[11], J S Haggerty[3], H Hamagaki[7], A G Hansen[19], H Hara[24], E P Hartouni[18], R Hayano[38], N Hayashi[31], X He[10], T K Hemmick[28], J M Heuser[28], M Hibino[41], J C Hill[13], D S Ho[43], K Homma[11], B Hong[15], A Hoover[26], T Ichihara[31,32], K Imai[17,31], M S Ippolitov[16], M Ishihara[31,32], B V Jacak[28,32], W Y Jang[15], J Jia[28], B M Johnson[3], S C Johnson[18,28], K S Joo[23], S Kametani[41], J H Kang[43], M Kann[30], S S Kapoor[2], S Kelly[8], B Khachaturov[42], A Khanzadeev[30], J Kikuchi[41], D J Kim[43], H J Kim[43], S Y Kim[43], Y G Kim[43], W W Kinnison[19], E Kistenev[3], A Kiyomichi[39], C Klein-Boesing[22], S Klinksiek[25], L Kochenda[30], V Kochetkov[12], D Koehler[25], T Kohama[11], D Kotchetkov[5], A Kozlov[42], P J Kroon[3], K Kurita[31,32], M J Kweon[15], Y Kwon[43], G S Kyle[26], R Lacey[27], J G Lajoie[13], J Lauret[27], A Lebedev[13,16], D M Lee[19], M J Leitch[19], X H Li[5], Z Li[6,31], D J Lim[43], M X Liu[19], X Liu[6], Z Liu[6], C F Maguire[40], J Mahon[3], Y I Makdisi[3], V I Manko[16], Y Mao[6,31], S K Mark[21], S Markacs[8], G Martinez[34], M D Marx[28], A Masaike[17], F Matathias[28], T Matsumoto[7,41], P L McGaughey[19], E Melnikov[12], M Merschmeyer[22], F Messer[28], M Messer[3], Y Miake[39], T E Miller[40], A Milov[42], S Mioduszewski[3,36], R E Mischke[19], G C Mishra[10], J T Mitchell[3], A K Mohanty[2], D P Morrison[3], J M Moss[19], F Mühlbacher[28], M Muniruzzaman[5], J Murata[31], S Nagamiya[14], Y Nagasaka[24], J L Nagle[8], Y Nakada[17], B K Nandi[5], J Newby[36], L Nikkinen[21], P Nilsson[20], S Nishimura[7], A S Nyanin[16], J Nystrand[20], E O'Brien[3], C A Ogilvie[13], H Ohnishi[3,11], I D Ojha[4,40], M Ono[39], V Onuchin[12], A Oskarsson[20], L Österman[20], I Otterlund[20], K Oyama[7,38], L Paffrath[3,*], A P T Palounek[19], V S Pantuev[28], V Papavassiliou[26], S F Pate[26], T Peitzmann[22], A N Petridis[13], C Pinkenburg[3,27], R P Pisani[3], P Pitukhin[12], F Plasil[29], M Pollack[28,36], K Pope[36], M L Purschke[3], I Ravinovich[42], K F Read[29,36], K Reygers[22],

[*] Deceased.

V Riabov[30,35], Y Riabov[30], M Rosati[13], A A Rose[40], S S Ryu[43], N Saito[31,32], A Sakaguchi[11], T Sakaguchi[7,41], H Sako[39], T Sakuma[31,37], V Samsonov[30], T C Sangster[18], R Santo[22], H D Sato[17,31], S Sato[39], S Sawada[14], B R Schlei[19], Y Schutz[34], V Semenov[12], R Seto[5], T K Shea[3], I Shein[12], T-A Shibata[31,37], K Shigaki[14], T Shiina[19], Y H Shin[43], I G Sibiriak[16], D Silvermyr[20], K S Sim[15], J Simon-Gillo[19], C P Singh[4], V Singh[4], M Sivertz[3], A Soldatov[12], R A Soltz[18], S Sorensen[29,36], P W Stankus[29], N Starinsky[21], P Steinberg[8], E Stenlund[20], A Ster[44], S P Stoll[3], M Sugioka[31,37], T Sugitate[11], J P Sullivan[19], Y Sumi[11], Z Sun[6], M Suzuki[39], E M Takagui[33], A Taketani[31], M Tamai[41], K H Tanaka[14], Y Tanaka[24], E Taniguchi[31,37], M J Tannenbaum[3], J Thomas[28], J H Thomas[18], T L Thomas[25], W Tian[6,36], J Tojo[17,31], H Torii[17,31], R S Towell[19], I Tserruya[42], H Tsuruoka[39], A A Tsvetkov[16], S K Tuli[4], H Tydesjö[,20], N Tyurin[12], T Ushiroda[24], H W van Hecke[19], C Velissaris[26], J Velkovska[28], M Velkovsky[28], A A Vinogradov[16], M A Volkov[16], A Vorobyov[30], E Vznuzdaev[30], H Wang[5], Y Watanabe[31,32], S N White[3], C Witzig[3], F K Wohn[13], C L Woody[3], W Xie[5,42], K Yagi[39], S Yokkaichi[31], G R Young[29], I E Yushmanov[16], W A Zajc[8], Z Zhang[28] and S Zhou[6]

[1]Institute of Physics, Academia Sinica, Taipei 11529, Taiwan
[2]Bhabha Atomic Research Centre, Mumbai 400 085, India
[3]Brookhaven National Laboratory, Upton, NY 11973-5000, USA
[4]Department of Physics, Banaras Hindu University, Varanasi 221005, India
[5]University of California – Riverside, Riverside, CA 92521, USA
[6]China Institute of Atomic Energy (CIAE), Beijing, People's Republic of China
[7]Center for Nuclear Study, Graduate School of Science, University of Tokyo, 7-3-1 Hongo, Bunkyo, Tokyo 113-0033, Japan
[8]Columbia University, New York, NY 10027; Nevis Laboratories, Irvington, NY 10533, USA
[9]Florida State University, Tallahassee, FL 32306, USA
[10]Georgia State University, Atlanta, GA 30303, USA
[11]Hiroshima University, Kagamiyama, Higashi-Hiroshima 739-8526, Japan
[12]Institute for High Energy Physics (IHEP), Protvino, Russia
[13]Iowa State University, Ames, IA 50011, USA
[14]KEK, High Energy Accelerator Research Organization, Tsukuba-shi, Ibaraki-ken 305-0801, Japan
[15]Korea University, Seoul 136-701, Korea
[16]Russian Research Center, Kurchatov Institute, Moscow, Russia
[17]Kyoto University, Kyoto 606, Japan
[18]Lawrence Livermore National Laboratory, Livermore, CA 94550, USA
[19]Los Alamos National Laboratory, Los Alamos, NM 87545, USA
[20]Department of Physics, Lund University, Box 118, SE-221 00 Lund, Sweden
[21]McGill University, Montreal, Quebec H3A 2T8, Canada
[22]Institut für Kernphysik, University of Münster, D-48149 Münster, Germany
[23]Myongji University, Yongin, Kyonggido 449-728, Korea
[24]Nagasaki Institute of Applied Science, Nagasaki-shi, Nagasaki 851-0193, Japan
[25]University of New Mexico, Albuquerque, NM 87131, USA
[26]New Mexico State University, Las Cruces, NM 88003, USA
[27]Chemistry Department, State University of New York – Stony Brook, Stony Brook, NY 11794, USA
[28]Department of Physics and Astronomy, State University of New York - Stony Brook, Stony Brook, NY 11794, USA
[29]Oak Ridge National Laboratory, Oak Ridge, TN 37831, USA
[30]PNPI, Petersburg Nuclear Physics Institute, Gatchina, Russia
[31]RIKEN (The Institute of Physical and Chemical Research), Wako, Saitama 351-0198, Japan
[32]RIKEN BNL Research Center, Brookhaven National Laboratory, Upton, NY 11973-5000, USA
[33]Universidade de São Paulo, Instituto de Física, Caixa Postal 66318, São Paulo CEP05315-970, Brazil

[34]SUBATECH, Ecole des Mines de Nantes, IN2P3/CNRS, Universite de Nantes, BP 20722-44307, Nantes Cedex 3, France
[35]St. Petersburg State Technical University, St. Petersburg, Russia
[36]University of Tennessee, Knoxville, TN 37996, USA
[37]Department of Physics, Tokyo Institute of Technology, Tokyo, 152-8551, Japan
[38]University of Tokyo, Tokyo, Japan
[39]Institute of Physics, University of Tsukuba, Tsukuba, Ibaraki 305, Japan
[40]Vanderbilt University, Nashville, TN 37235, USA
[41]Advanced Research Institute for Science and Engineering, Waseda University, 17 Kikui-cho, Shinjuku-ku, Tokyo 162-0044, Japan
[42]Weizmann Institute, Rehovot 76100, Israel
[43]Yonsei University, IPAP, Seoul 120-749, Korea
[44]KFKI Research Institute for Particle and Nuclear Physics (RMKI), Budapest, Hungary[†]

1. Introduction

PHENIX is one of the five experiments at the recently commissioned RHIC collider at Brookhaven National Laboratory. During the year 2000 first data with gold beams were taken at a center-of-mass energy of 130 GeV. PHENIX accumulated a sample of approximately 2×10^6 minimum bias $\mathrm{Au} + \mathrm{Au}$ collisions. In this paper I will highlight some of the many results that have emerged from this sample. Other papers at this conference [1–3] will go into more depth for specific topics and address results like two-particle correlations [4] and event-by-event fluctuations not covered in this summary.

2. The PHENIX detector

The PHENIX detector is designed to measure penetrating probes, specifically direct photon radiation, heavy flavor, and jet production. These probes are especially suited to study the early stages of high energy heavy-ion collisions where quark matter is expected to form. Over a limited angular acceptance PHENIX combines excellent momentum resolution, lepton identification, and electromagnetic calorimetry with a high rate capability. In addition, in the mid-rapidity region PHENIX can address a wide range of other observables, for example light vector mesons, in particular the ϕ in its decay modes to kaons and electrons, inclusive single hadron and hadron pair spectra, as well as many global characteristics of the collision.

PHENIX is composed of four arms. Two central arms are dedicated to electron and photon measurements in combination with hadronic observables each covering 90 degree in azimuthal angle and ± 0.35 in pseudo-rapidity η around mid-rapidity. In forward and backward region between 1.15 and 2.25 in $|\eta|$, muons are measured with full azimuthal coverage.

During the run in 2000 only parts of both central arms were operational. Figure 1 gives a schematic overview. Neutral pions are reconstructed from the invariant mass distribution of

[†]Not a participating institution.

photon pairs. Transverse energy and photons are measured independently in two different systems, two sectors of lead scintillator (PbSc) calorimeter on the west arm and one sector of lead glass (PbGl) calorimeter on the east side, with each sector covering 1/8 of the azimuthal acceptance. In the east arm, trajectories and momenta of charged hadrons are measured with a drift chamber (DC) and two MWPCs with pad readout (PC1 and PC3). Pions, kaons and protons are identified by time of flight (ToF) within half of the azimuthal acceptance of the east arm. In the west arm charged particles are reconstructed with the DC and PC1. Among these, electrons can be identified by combining information from a ring imaging Cherenkov counter with energy and momentum measurements.

In addition, lead glass beam–beam counters (BBC) covering 3.1 to 3.9 in $|\eta|$ and zero degree calorimetry (ZDC) allow event characterization.

3. Global observables

PHENIX has recorded minimum bias Au–Au events corresponding to ∼92% of the nuclear interaction cross-section. For most analyses the events are grouped in fractions of the cross-section according to centrality. The classification is based on the combined BBC-ZDC information. For each class the average number of participating nucleons $N_{\rm part}$ and binary nucleon–nucleon collisions $N_{\rm binary}$ is determined with a Glauber-model based MC method, which includes the BBC and ZDC detector resolutions.

Figure 2 shows the transverse energy $E_{\rm T}$ determined from two sectors of the PbSc calorimeter covering 45° in azimuth [5]. Two axis are shown, the top gives the measured transverse energy, and the bottom one the fully corrected transverse energy scaled to 2π azimuthal coverage. The average transverse energy for the most central 2% of the interaction cross section is $\mathrm{d}E_{\rm T}/\mathrm{d}\eta = 578 + 26 - 39$ GeV. Using the Bjorken estimate to relate $E_{\rm T}$ to the initial energy density we find $\varepsilon\tau_0 = 4.6$ GeV/c fm^2. This is a factor ∼1.6 larger than in Pb–Pb collisions at SPS energies [6]. With a reasonable choice of the formation time τ_0 we find the initial energy density to be 5–20 GeV/fm^3 .

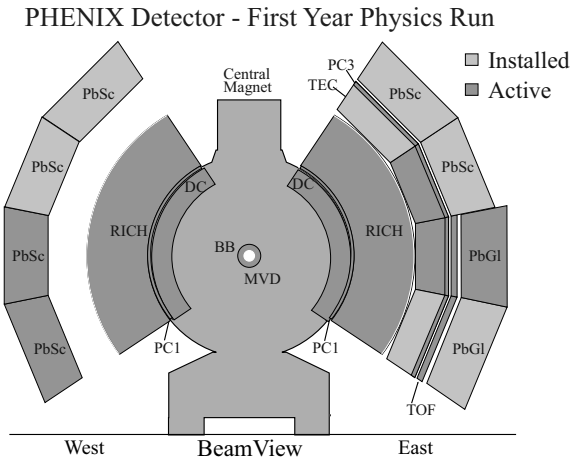

Figure 1. PHENIX setup used during the first RHIC run.

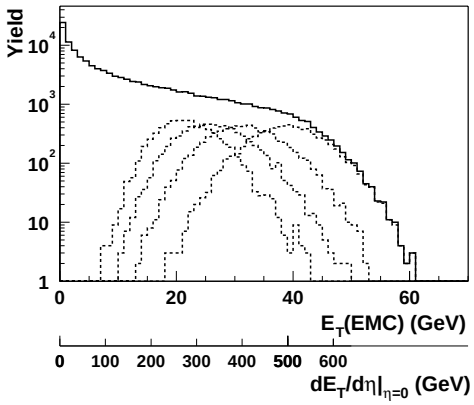

Figure 2. Transverse energy distribution from Au–Au collisions. The dashed curves correspond to four centrality selections of 5% cross-section each, i.e., 0–5%, 5–10%,10–15% and 15–20%.

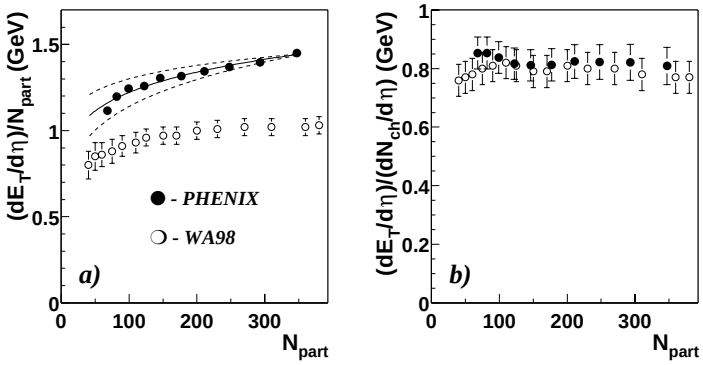

Figure 3. The left panel gives the transverse energy density produced per participant. The dashed lines indicate the systematic errors relative to central collisions. The left plot shows the centrality dependence of E_T per charged particle. Both panel show the WA98 [7] data for comparison.

With increasing E_T also more particles are produced [8]. As indicated in the left panel of figure 3, the average charge particle multiplicity seems to be proportional to E_T, both with centrality and center-of-mass energy, which indicates universal conditions for particle production.

The E_T production (left panel of figure 3) as well as the charged-particle production (figure 4) per participant increases with centrality. This increase has been reproduced equally well in a two-component model with soft and hard particle production [9] and in the framework of gluon saturation [10].

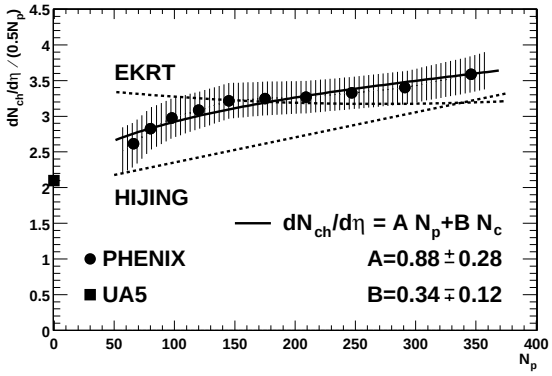

Figure 4. Charged particle density per participant pair as a function of centrality. The band indicates the systematic errors.

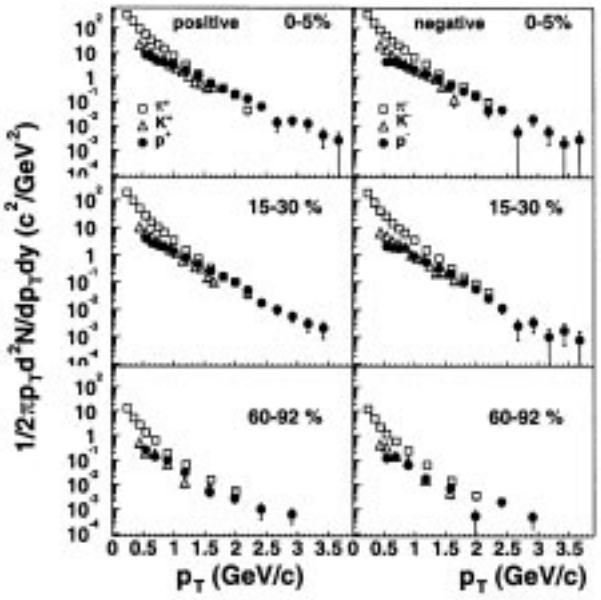

Figure 5. Transverse momentum spectra for identified charged particles for different centrality selections.

4. Hadron yields and spectra

PHENIX has published spectra of charged pions, kaons, protons and their anti-particles over a broad p_{T} range [1,11]. Figure 5 shows the measured p_{T} distribution for different centrality selections. They are discussed in detail in [1]. In central collisions the proton and anti-proton yields become comparable to the pion yields around 2 GeV/c. Most commonly this is interpreted in the context of thermal models as indication for substantial radial flow [12,13]. Alternative explanations are initial-state gluon saturation that results in m_{T} scal-

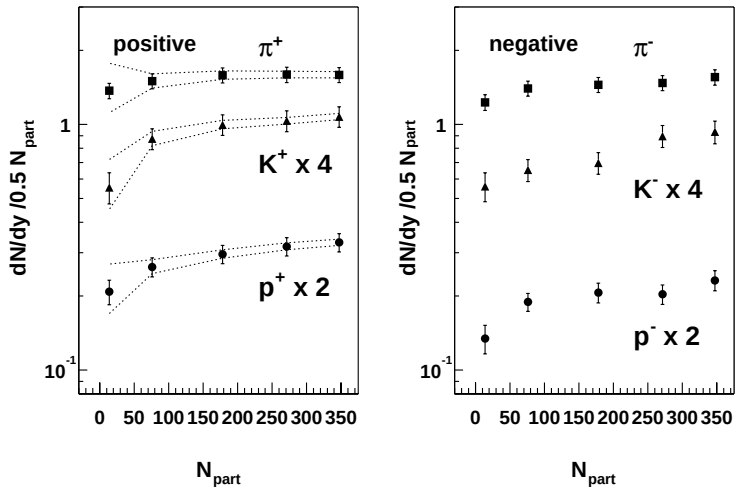

Figure 6. Centrality dependence for identified charged particle densities.

ing [14] or proton/anti-proton production via gluon-junctions combined with quenching of pion production [15].

Figure 6 shows the integrated yields extrapolated to all p_{T} as a function of centrality. For peripheral collisions the yields extrapolate back to the values from pp and $\bar{p}p$ data. The yields of all particle increase rapidly until about $N_{\mathrm{part}} \sim 100$, corresponding to 10 fm impact parameter. For more central collisions the pion yield scales with N_{part} while kaon, proton, and anti-proton yields continue to increase faster than N_{part}.

The yields of particles and anti-particles are very similar, indicating that most particles are produced during the collision. In particular, the number of produced protons and anti-protons is large. While the net proton density, measured as the density of protons minus anti-protons, is only about 9 in central collisions, the total density of protons plus anti-protons is almost 50. Assuming isospin symmetry and ignoring hyperons the baryon plus anti-baryon density is $\sim$100, roughly 10% larger than at the SPS [16]. Including a correction for hyperons will increase the baryon plus anti-baryon density at RHIC well beyond that observed at the SPS. The large number of baryons and anti-baryons at mid-rapidity has important consequences for calculations of in-medium modifications of hadron properties [17]. Unlike the original expectation, density effects cannot be neglected at RHIC. In fact similar conditions for medium modifications are created at RHIC and at the SPS.

5. High p_{T} phenomena

Hard scattering provides a novel tomographic tool to study nuclear matter created in heavy-ion collisions at collider energies. In pp collisions at similar energies a substantial fraction of hadrons with p_{T} above 2 GeV/c results from jet production. In the absence of nuclear effects in Au–Au collisions hadron yields at high p_{T} should increase proportional to N_{binary}. It has been predicted theoretically that in dense quark matter hard scattered partons lose

energy via gluon bremsstrahlung [18], effectively quenching jet production and thus high p_T particle production.

PHENIX discovered that in central collisions both the yield of charged hadrons and of neutral pions is suppressed compared to binary scaling [19]. Figure 7 shows the comparison of the spectra of charged particles and neutral pions produced in central and peripheral Au–Au collisions. While in peripheral collisions the yields follow the binary scaling extrapolation reasonably well, in central collisions the hadron yields are significantly suppressed. This suppression is quantified in figure 8 by the nuclear modification factor R_{AA}, i.e., the ratio of Au–Au data to the extrapolation.

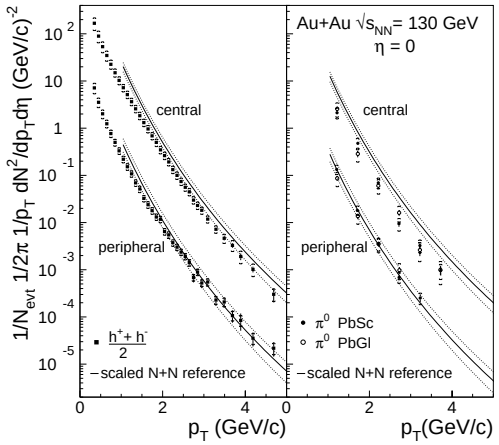

Figure 7. Invariant cross-sections for charged hadrons and neutral pions. All data sets are compared to binary scaling of the nucleon–nucleon distribution.

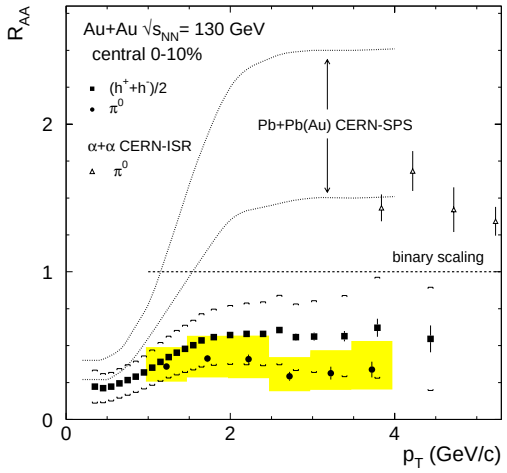

Figure 8. Nuclear modification factor for central collisions compared to data from lower energies.

Above 2 GeV/c, R_{AA} remains significantly below unity. The factor of 1.5 difference between charged hadrons and neutral pions reflects the larger proton plus anti-proton contribution to the charged particle spectra discussed earlier which is larger than what was observed at the ISR. R_{AA} is also below Pb–Pb data from the SPS as well as $\alpha\alpha$ data from the ISR, both measured at lower energies where the production of high p_{T} hadrons is enhanced. This enhancement is commonly referred to as Cronin effect, and has been interpreted in terms of initial state multiple scattering.

The observed suppression indicates the absence of the expected hard scattering contribution. The suppression is consistent with jet quenching due to gluon bremsstrahlung [9]. However, this interpretation is not unique. Initial state gluon saturation which leads to m_{T} scaling [14] as well as thermal models with radial flow [12,13] also explain the central data. More information is needed to discriminate models, in particular data at higher p_{T}.

For charged-particle production a systematic study of the centrality dependence is available. We have calculated R_{AA} for five centrality classes: 0–5%, 5–15%, 15–30%, 30–60%, and 60–80% (figure 9). For peripheral collisions R_{AA} increases monotonically, which is similar to the expected Cronin effect. With increasing centrality, R_{AA} decreases for all p_{T}, but above 2 GeV/c it decreases faster as p_{T} gets larger. If the suppression is quantified as deviation of R_{AA} from peripheral collisions, we find that the suppression increases with centrality and p_{T}.

To underline the characteristic centrality dependence we calculate R_{AA} for three large p_{T} bins and plot it as a function of centrality (figure 10). For all p_{T} bins, R_{AA} decreases with centrality, but it decreases faster for larger p_{T}. Evidently the yield of high p_{T} particles does not scale with N_{binary}. To test a different scaling assumption we have recalculated R but normalized to N_{part}, i.e., $R = \mathrm{yield}(AA)/\mathrm{yield}(pp)/N_{\mathrm{part}}$. The result is given in the bottom panel of the figure. The high p_{T} yield does not scale with N_{part} either. However, above $N_{\mathrm{part}} = 100$ the deviations from simple scaling are small. The data clearly indicate the absence of the expected contribution of hard scattering for collisions involving more than $\sim$100 participants.

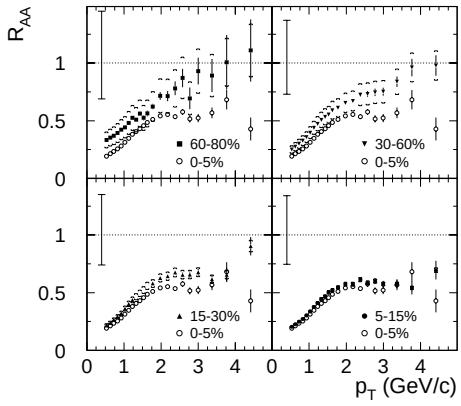

Figure 9. R_{AA} for charged particles from 5 different centrality selection. The common relative systematic error on the scale is plotted as bar around unity in the upper left panel. The systematic uncertainty of each set relative to the most central one, which results mostly from N_{part}, are given as brackets.

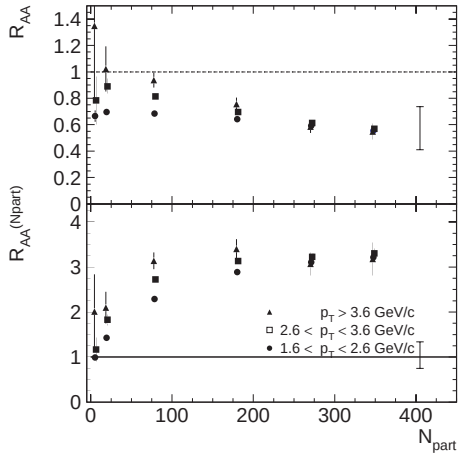

Figure 10. Particle yields for exclusive p_{T}-bins normalized to N_{binary} (top) or N_{part} (bottom).

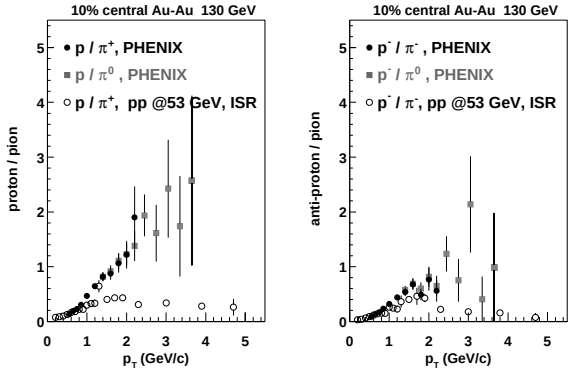

Figure 11. Ratio of protons (left) and anti-protons (right) to charged and neutral pions form central Au–Au collisions. For comparison the figure also shows data from pp collisions taken at the ISR.

A method to search for the transition from soft- to hard-particle production is provided by the p_{T} dependence of p/π [20]. Soft-particle production described by m_{T} scaling or thermal distributions plus radial flow leads to an increasing p/π ratio which saturates at high p_{T}. In contrast, hard scattering will lead to a decreasing ratio due to the different valence quark contributions. Thus the p_{T} at which the trend changes from a rising to a falling p/π ratio can be interpreted as transition from soft to hard processes dominating particle production. For central collisions the measured ratios p/π and $\bar{p}/\pi$ are shown in figure 11 together with the ISR results [21]. The transition point can be fixed to about 1.8 GeV/c at ISR energies. In central Au–Au collisions both ratios increase with p_{T} up to 3.5 GeV/c, indicating no evidence for hard scattering.

6. Electron yields and heavy flavor

PHENIX has also measured inclusive single electron plus positron spectra in the p_{T} range from 0.2 to 3.0 GeV/c [22]. Most electrons result from decays of light mesons, such as π° and η Dalitz decays, and from photon conversions. Their contribution has been estimated based on the measured charged and neutral π spectra. Figure 12 shows the electron p_{T} spectra from a minimum bias and a central event selection after the contribution from light meson decays and photon conversions was subtracted. Also shown in the figure are estimates based on Pythia calculations of the contribution from semi-leptonic decays of hadrons with open charm or beauty shown in the figure are determined using Pythia, which was tuned to describe existing data on charm production. Also shown is an estimate of direct radiation [23]. Electrons from decays of charmed mesons dominate the remaining sample below 3 GeV/c.

In turn we use our data to estimate the charm cross-section assuming all electrons in figure 12 originate from charm decays. We divide the obtained cross-section by N_{binary}. The result is 420 ± 250 μb for the minimum bias sample. In figure 13 our estimate

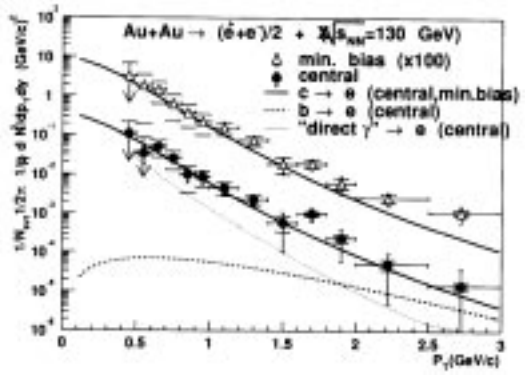

Figure 12. Inclusive electron distribution after subtraction of the decay contribution from light meson. For comparison we show the expected contribution from open charm and beauty, as well as an estimate of thermal radiation.

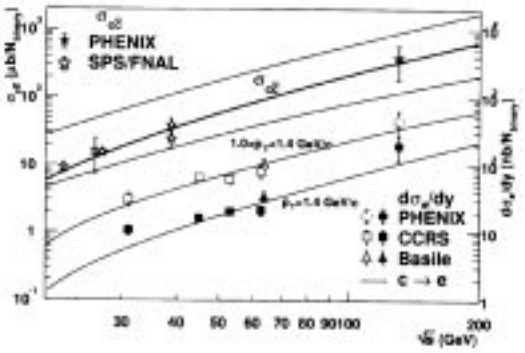

Figure 13. Compilation of charm cross-section measurements as a function of $\sqrt{s}$. Also shown are data on inclusive electron production, after background subtraction.

is compared to lower energy data and the expected $\sqrt{s}$ dependence for first- and second-order QCD calculations is given by the solid line and the shaded band respectively. A good agreement of our data with the expectation from binary scaling leaves little room for large suppression or enhancement of the charm cross-section in heavy ion collisions.

Acknowledgements

We thank the staff of the Collider-Accelerator and Physics Departments at BNL for their vital contributions. We acknowledge support from the Department of Energy and NSF (USA), Monbu-sho and STA (Japan), RAS, RMAE, and RMS (Russia), BMBF, DAAD, and AvH (Germany), VR and KAW (Sweden), MIST and NSERC (Canada), CNPq and FAPESP (Brazil), IN2P3/CNRS (France), DAE and DST (India), KRF and CHEP (Korea), the US CRDF for the FSU, and the US-Israel BSF.

References

[1] J Velkovska, PHENIX collaboration, *Pramana – J. Phys.* **60** (2003)
[2] D Silvermyr, PHENIX collaboration, *Pramana – J. Phys.* **60** (2003)
[3] J P Sullivan, PHENIX collaboration, *Pramana – J. Phys.* **60** (2003)
[4] K Adcox *et al*, PHENIX collaboration, nucl-ex/0201008
[5] K Adcox *et al*, PHENIX collaboration, *Phys. Rev. Lett.* **87**, 052301 (2001)
[6] T Alber *et al*, NA49, *Phys. Rev. Lett.* **75**, 3814 (1995)
[7] M M Aggarwal *et al*, *Euro. Phys. J.* **C18**, 651 (2001)
[8] K Adcox *et al*, PHENIX collaboration, *Phys. Rev. Lett.* **86**, 3500 (2001)
[9] X N Wang and M Gyulassy, *Phys. Rev. Lett.* **86**, 3496 (2001)
[10] D Kharzeev and M Nardi, *Phys. Lett.* **B507**, 121 (2001)
[11] K Adcox *et al*, PHENIX collaboration, nucl-ex/0112006
[12] D Teaney, J Lauret and E V Shuryak, nucl-th/0110037
[13] P Kolb *et al*, *Nucl. Phys.* **A696**, 197 (2001)
[14] J Schaffner-Bielich *et al*, *Nucl. Phys. A* (in print); nucl-th/0108048
[15] I Vitev *et al*, nucl-th/0104066
[16] I Tserruya, *Pramana – J. Phys.* **60**, 639 (2003)
[17] R Rapp, *Phys. Rev.* **C63**, 54907 (2001)
[18] M Gyulassy and M Plümer, *Phys. Lett.* **B243**, 432 (1990)
X N Wang and M Gyulassy, *Phys. Rev. Lett.* **68**, 1480 (1992)
R Baier *et al*, *Phys. Lett.* **B345**, 277 (1995)
[19] B Alper *et al*, *Nucl. Phys.* **100**, 237 (1975)
[20] K Adcox *et al*, PHENIX collaboration, *Phys. Rev. Lett.* **88**, 22301 (2002)
[21] W M Geist *et al*, *Phys. Rep.* **197**, 263 (1990)
[22] K Adcox *et al*, PHENIX collaboration, nucl-ex/0202002
[23] J Alam *et al*, hep-ph/0008074